International Journal of
INTELLIGENT SYSTEMS AND APPLICATIONS IN ENGINEERING
ISSN:2147-6799 www.ijisae.org Original Research Paper

# ADRC controller for buck converter - inverter system for photovoltaic applications

**Esteva Pérez, R[1], Guerrero Ramírez, E. O*[2], Contretas Ordaz, M. A[3]**

**Submitted:** 12/01/2025 **Revised:** 22/02/2025 **Accepted:** 03/03/2025

**Abstract:** This paper presents the design and simulation of the Active Disturbance Rejection Control (ADRC) for a buck-boost converter-inverter system powered by photovoltaic panels. The system features a two-stage configuration, based on a buck-type DC/DC converter and a single-phase inverter, connected in cascade. The objectives of this work are the voltage regulation at the output of the buck converter and the sinusoidal current tracking at the output of the inverter. Active Disturbance Rejection Control is employed from the perspective of differential flatness and Generalized Proportional Integral (GPI) extended state observers. The simulations of the proposed photovoltaic system are carried out in the MATLAB/Simulink environment. Additionally, to evaluate the performance of the photovoltaic system and the robustness of the controller, simulation results are presented under input voltage variations and load disturbances. Furthermore, Total Harmonic Distortion (THD) graphs of the sinusoidal current at the output of the inverter are provided. The simulation results demonstrate appropriate behavior of the Active Disturbance Rejection Control, as evidenced by a short settling time of the buck converter and accurate current reference tracking.

***Keywords:*** *ADRC controller, Buck converter, Inverter, Photovoltaic*

## 1. Introduction

One of the promising alternatives to non-renewable energy is converting solar energy into electrical energy through photovoltaic (PV) cells. These are electronic devices that use a process called the photovoltaic effect. Photovoltaic cells have a solar-to-electric conversion efficiency ranging from 17% to 24%. However, this electrical conversion is not fully optimized due to the non-linear behavior of the voltage-current and voltage-power curves, which depend on variables such as irradiance and the temperature of the photovoltaic cells. Figure 1 shows the behavior of these curves at an irradiance level of 1000 W/m² under different operating temperatures, while Figure 2 displays the curves considering different irradiance levels at a fixed cell temperature of 25°C.
In both cases, it can be observed that the Maximum Power Point (MPP) varies according to the operating conditions, and this value changes if the independent variables do not remain under the same conditions.

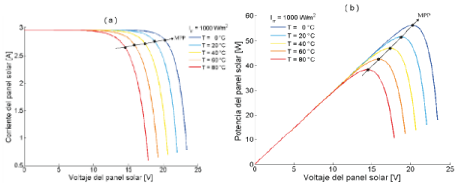


Figure 1. Curves: a) Voltage versus current and b) Voltage versus power, with constant irradiance Irr = 1000 W/m².

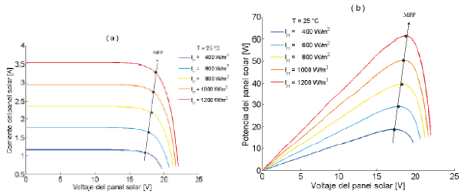


Figure 2. Curves: a) Voltage versus current and b) Voltage versus power, with a constant temperature T = 25°C.

This work proposes a two-stage configuration consisting of a DC/DC buck converter cascaded with an inverter. The DC/DC converter is connected to the photovoltaic cells to achieve voltage regulation, while the inverter is responsible for current tracking. Both stages utilize the Active Disturbance Rejection Control (ADRC) technique to achieve regulation and tracking, despite the varying conditions that may arise in the photovoltaic cells and the load.

## 2. Design of the Photovoltaic System

A crucial problem in photovoltaic systems is that variations in the input source or the load lead to a variable output voltage or current, which is detrimental to any system. This highlights the need to utilize an appropriate control technique to counteract these effects of instability and potential damage to the system.

*1 National Technological Institute of Mexico, National Center for Research and Technological Development (TECNM/CENIDET) -MEXICO*
*2 Technological University of the Mixteca (UTM) - MEXICO*
*3 Technological University of the Mixteca (UTM) – MEXICO*
* *Corresponding Author Email: roosemvelt99@gmaill.com*

One solution is the proposed system in Figure 3, which includes the connection of a buck converter and an inverter. The DC/DC buck converter aims to regulate the input voltage supplied by the solar panels, while the inverter seeks to achieve accurate tracking of a desired current, both utilizing the ADRC technique. This controller is chosen because it will help actively reject the endogenous and exogenous disturbances in the system.

The flat outputs of voltage and current are fed into the Active Disturbance Rejection Control, from which the control signals are obtained and compared with triangular signals to assist in the switching of the switches.

The cascade connection of the photovoltaic cells and the power electronic converters results in a system that is quite complex to analyze due to the large number of variables involved.

Based on the mathematical model, the property of differential flatness, and ADRC, the controller for the photovoltaic system is designed. For the controller design, it is essential to measure the flat outputs of the system. A PWM modulation is used to control the power devices of the buck-type DC/DC converter, and a bipolar PWM modulation is proposed for the inverter.

The mathematical analysis was developed by applying Kirchhoff's current and voltage laws to the photovoltaic system, resulting in the system of equations (10), which are used for the design of the ADRC controller [14].

$$L \cdot \frac{di}{dt} = Eu_1 - V_C$$

$$C \cdot \frac{dv_c}{dt} = i_L + (1 - 2u_2)i_0 \quad (10)$$

$$L_0 \cdot \frac{di_0}{dt} = -(1 - 2u_2)V_C - i_0(R_0 + R_c)$$

Where $u_1, u_2 \in [0, 1]$

- ***u₁:*** *Control signal for the buck converter*
- ***u₂:*** *Control signal for the inverter*
- ***E:*** *Input voltage*
- ***C:*** *Capacitor of the buck converter*
- ***L:*** *Inductor of the buck converter*
- ***L₀:*** *Load inductor*
- ***R₀:*** *Series resistance associated with the load inductor*
- ***Rₗ:*** *Load resistance*
- ***iₗ:*** *Current in the inductor of the buck converter*
- ***Vₕ:*** *Voltage across the capacitor*
- ***i₀:*** *Output current of the invertir*

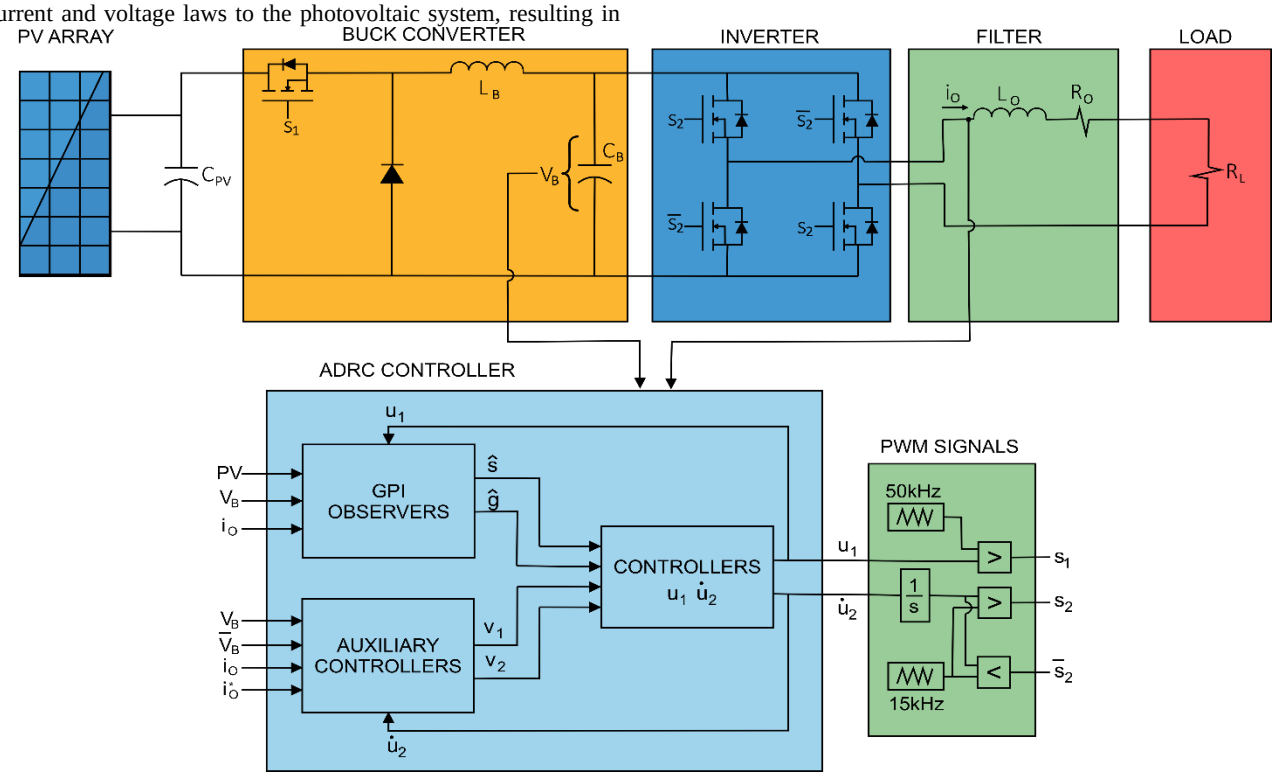


Figure 3. Active Disturbance Rejection Control of the Photovoltaic System.

## 3. Design of Active Disturbance Rejection Control (ADRC)

Considering the system of equations (10) resulting from the developed photovoltaic system, the design of the ADRC for the photovoltaic system is carried out.

By considering the system of equation (10) and performing a change of variables $x_1 = i_L$, $x_2 = v_C$ y $x_3 = i_0 = I_0$, the system described by equation (11) is obtained.

By inspecting the resulting equations of the system, it is observed that it is a flat system, whose flat outputs are $x_2 = v_C$ y $x_3 = i_0$, responsible for the parameterization of the system.

$$L \cdot \frac{di}{dt} = Eu_1 - x_2$$

$$C \cdot \frac{dv_c}{dt} = x_1 + (1 - 2u_2)x_3 \quad (11)$$

$$L_0 \cdot \frac{di_0}{dt} = -(1 - 2u_2)x_2 - x_3(R_0 + R_c)$$

Since the number of control inputs must equal the number of flat outputs, there are two control inputs and two flat outputs [15]. In the system of equation (12), the differential parameterization is shown, which consists of expressing the state variables and the control inputs in terms of the flat outputs FFF and their derivatives.

$$x_1 = C\dot{F}_1 + \frac{L_O F_2 \dot{F}_2}{F_1} + \frac{F_2^2(R_O + R_C)}{F_1}$$

$$x_2 = F_1 \quad (12)$$

$$x_3 = F_2$$

In equation (13), the control signals are shown, which are expressed in terms of the higher-order derivatives of the flat outputs $\ddot{F}_1$ and $\ddot{F}_2$, where $\phi_1$ and $\phi_2$ are considered the internal and external disturbances affecting the system.

The relationship that links the control inputs with the higher-order derivatives through a matrix turns out to be non-invertible. This indicates that the relative degree is not well defined; hence, a dynamic extension of the control input $u_2$ leads to a well-defined relative degree according to the selected inputs and flat outputs [15]. This relationship is shown in equation (13).

$$
\begin{aligned}
u_1 &= \frac{L\,C}{E}\ddot{F}_1 + \frac{LL_OF_2}{EF_1}\ddot{F}_2 + \phi_1 \\
\dot{u}_2 &= \frac{L_O}{2F_1}\ddot{F}_2 + \phi_2 \\
\phi_1 &= \frac{2LF_2}{EF_1}\big((R_O + R_C)\big)\dot{F}_2 + LL_O\frac{F_1\dot{F}_2\dot{F}_2}{EF_1^2} \\
&-LL_O\frac{F_2\dot{F}_1\dot{F}_2}{EF_1^2} - L(R_O + R_C)\left(\frac{F_2^2\dot{F}_1}{EF_1^2}\right) + \frac{F_1}{E} \\
\phi_2 &= -\frac{L_O\dot{F}_2\dot{F}_1}{2F_1^2} + \frac{(R_O + R_C)F_1\dot{F}_2}{2F_1^2} \\
&\quad - \frac{(R_O + R_C)F_2\dot{F}_1}{2F_1^2}
\end{aligned}
\tag{13}
$$

Equation (13) is expressed in matrix form, as shown in equation (14).

$$
\begin{pmatrix} u_1 \\ \dot{u}_2 \end{pmatrix} = \begin{pmatrix} \frac{LC}{E} & \frac{LL_OF_2}{EF_1} \\ 0 & \frac{L_O}{2F_1} \end{pmatrix}\begin{pmatrix} \ddot{F}_1 \\ \ddot{F}_2 \end{pmatrix} + \begin{pmatrix} \phi_1 \\ \phi_2 \end{pmatrix} \tag{14}
$$

By isolating the higher-order derivatives of the flat outputs $\ddot{F}_1$ and $\ddot{F}_2$ from equation (14), equation (15) is obtained.

$$
\begin{aligned}
\begin{pmatrix} \ddot{F}_1 \\ \ddot{F}_2 \end{pmatrix} &= \begin{pmatrix} \frac{E}{LC} & -\frac{2F_2}{C} \\ 0 & \frac{2F_1}{L_O} \end{pmatrix}\begin{pmatrix} u_1 \\ \dot{u}_2 \end{pmatrix} \\
&\quad - \begin{pmatrix} \frac{E}{LC} & -\frac{2F_2}{C} \\ 0 & \frac{2F_1}{L_O} \end{pmatrix}\begin{pmatrix} \phi_1 \\ \phi_2 \end{pmatrix} \\
\begin{pmatrix} \ddot{F}_1 \\ \ddot{F}_2 \end{pmatrix} &= \begin{pmatrix} \frac{E}{LC} & -\frac{2F_2}{C} \\ 0 & \frac{2F_1}{L_O} \end{pmatrix}\begin{pmatrix} u_1 \\ \dot{u}_2 \end{pmatrix} + \begin{pmatrix} \varphi_1 \\ \varphi_2 \end{pmatrix}
\end{aligned}
\tag{15}
$$

In equation (16), the GPI voltage observer is shown in terms of the flat output $F_1$, which includes an integrator for a more suitable approximation of the observer.

$$
\begin{aligned}
\dot{\hat{F}}_1 &= \hat{F}_{C1} + \lambda_2(F_1 - \hat{F}_1) \\
\dot{\hat{F}}_{C1} &= \left(\frac{E}{LC}\right)u_1 - \frac{2F_2}{C}\dot{u}_2 + \hat{s}_1 + \lambda_1(F_1 - \hat{F}_1) \\
\dot{\hat{s}}_1 &= \lambda_0\big(F_1 - \hat{F}_1\big)
\end{aligned}
\tag{16}
$$

Considering that $v_C = F_1$ and $\hat{s}_1 = \varphi_1$, equation (17) is obtained.

$$
\begin{aligned}
\dot{\hat{v}}_C &= \hat{v}_{C1} + \lambda_2(v_C - \hat{v}_C) \\
\dot{\hat{v}}_{C1} &= \left(\frac{E}{LC}\right)u_1 - \frac{2I_0}{C}\dot{u}_2 + \hat{s}_1 + \lambda_1(v_C - \hat{v}_C) \\
\dot{\hat{s}}_1 &= \lambda_0(v_C - \hat{v}_C)
\end{aligned}
\tag{17}
$$

In equation (18), the GPI current observer is shown in terms of the flat output $F_2$, which includes an integrator for a more suitable approximation.

$$
\begin{aligned}
\dot{\hat{F}}_2 &= \hat{F}_{O2} + \delta_2\big(F_2 - \hat{F}_2\big) \\
\dot{\hat{F}}_{O2} &= \frac{2F_1}{L_O}\dot{u}_2 + \hat{g}_1 + \delta_1\big(F_2 - \hat{F}_2\big) \\
\dot{\hat{g}}_1 &= \delta_0\big(F_2 - \hat{F}_2\big)
\end{aligned}
\tag{18}
$$

Considering that $I_O = F_2$ and $\hat{g}_1 = \varphi_2$, equation (19) is obtained.

$$
\begin{aligned}
\dot{\hat{I}}_0 &= \hat{I}_{O1} + \delta_2\big(I_O - \hat{I}_O\big) \\
\dot{\hat{I}}_{O1} &= \frac{2V_c}{L_O}\dot{u}_2 + \hat{g}_1 + \delta_1\big(I_O - \hat{I}_O\big) \\
\dot{\hat{g}}_1 &= \delta_0\big(I_O - \hat{I}_O\big)
\end{aligned}
\tag{19}
$$

To tune the coefficients $\lambda$ and $\delta$ of the proposed GPI voltage and current observers, the pole placement method is used. For this case, the following third-order Routh-Hurwitz polynomial is chosen: $P_1 = (s^2 + (2\zeta_1\omega_{n1})s + \omega_{n1}^2)(s + \alpha) = P_2$. The tuning of the observers is represented in the set of equations (20) and (21). For the damping coefficients $\zeta_{1,}, \zeta_{11}$, the values must be specified within $0 < \zeta_1, \zeta_{11} < 1$, and the system frequency must be within $0 < \omega_{n1,}\omega_{n11}$, with $\alpha > 0$.

Tuning of the voltage observer:

$$
\begin{aligned}
P_1 &= s^3 + s^2(2\zeta_1\omega_{n1} + \alpha) + s(\omega_{n1}^2 + 2\zeta_1\omega_{n1}\alpha) \\
&\quad + \alpha\omega_{n1}^2 \\
\lambda_O &= \alpha\omega_{n1}^2 \\
\lambda_1 &= \omega_{n1}^2 + 2\zeta_1\omega_{n1}\alpha \\
\lambda_2 &= 2\zeta_1\omega_{n1} + \alpha
\end{aligned}
\tag{20}
$$

Sintonización del observador de corriente:

$$
\begin{aligned}
P_2 &= s^3 + s^2(2\zeta_{11}\omega_{n11} + \alpha) \\
&\quad + s(\omega_{n11}^2 + 2\zeta_{11}\omega_{n11}\alpha) \\
&\quad + \alpha\omega_{n11}^2 \\
\delta_O &= \alpha\omega_{n11}^2 \\
\delta_1 &= \omega_{n11}^2 + 2\zeta_{11}\omega_{n11}\alpha \\
\delta_2 &= 2\zeta_{11}\omega_{n11} + \alpha
\end{aligned}
\tag{21}
$$

In equations (22) and (23), auxiliary controllers $v_1$ and $v_2$ are used to achieve the desired behavior of voltage regulation and current tracking of the desired flat outputs $\bar{v}_C$ y $I_O^*$.

Design of the auxiliary voltage controller $v_1$:

$$
\begin{aligned}
v_1 &= \ddot{F}_1^* - k_1\big(\hat{F}_1 - \dot{F}_1^*\big) - k_0(F_1 - F_1^*) \\
v_1 &= -k_1\big(\hat{F}_1\big) - k_0(F_1 - F_1^*) \\
v_1 &= -k_1\hat{v}_{C1} - k_0(v_C - \bar{v}_C)
\end{aligned}
\tag{22}
$$

Design of the auxiliary current controller $v_2$:

$$
\begin{aligned}
v_2 &= \ddot{F}_2^* - k_1\big(\hat{F}_2 - \dot{F}_2^*\big) - k_0(F_2 - F_2^*) \\
v_2 &= \ddot{I}_O^* - k_3\big(\hat{I}_{O1} - \dot{I}_{O1}^*\big) - k_2(I_O - I_O^*)
\end{aligned}
\tag{23}
$$

For the coefficients $k_0, k_1, k_2, k_3$ of the auxiliary controllers, the second-order Routh-Hurwitz polynomial $P_3 = s^2 + (2\zeta_2\omega_{n2})s + \omega_{n2}^2 = P_4$ was used. The tuning of the coefficients is expressed in equations (24) and (25), where $0 < \zeta_2, \zeta_3 < 1$ and $\omega_{n2}, \omega_{n3} > 0$.

Tuning of the auxiliary voltage controller $v_1$:

$$
\begin{aligned}
P_3 &= s^2 + (2\zeta_2\omega_{n2})s + \omega_{n2}^2 \\
k_0 &= \omega_{n2}^2
\end{aligned}
\tag{24}
$$

$$k_1 = 2\zeta_2\omega_{n2}$$

Tuning of the auxiliary current controller $v_2$:

$$P_4 = s^2 + (2\zeta_3\omega_{n3})s + \omega_{n3}^2$$
$$k_2 = \omega_{n3}^2 \quad (25)$$
$$k_3 = 2\zeta_3\omega_{n3}$$

In equation (26), the mathematical design of the desired sinusoidal signal is shown..

$$I_O^* = A\ \sin(\omega_n t)$$
$$I_{O1}^* = \dot{I}_O^* = A\ \omega_n \cos(\omega_n t) \quad (26)$$
$$\dot{I}_{O1}^* = \ddot{I}_O^* = -A\ (\omega_n)^2 \sin(\omega_n t)$$

Finally, in equation (27), the control for each of the inputs is shown, where the control signal $u_2$ is obtained by integrating $\dot{u}_2$.

$$u_1 = \frac{LC}{E}(v_1 - \hat{s_1}) + \frac{LL_O I_O}{EF_1}(v_2 - \hat{g}_1) \quad (27)$$
$$\dot{u}_2 = \frac{L_O}{2v_C}(v_2 - \hat{g}_1)$$

## 4. Modeling of Solar Panels in MATLAB/Simulink

The characteristics of the EPCOM PRO-5012 Photovoltaic Solar Panel [16] are shown in Table 1. Since each panel provides a power of 50 W, ten panels will be connected in series to obtain a DC voltage of approximately 179 V, with a power of 500 W and a current of 2.79 A, according to the characteristics outlined in Table 1. Using the DC/DC buck converter, the voltage provided by the solar panels will be reduced to 160 V, which will be used to power the inverter circuit. With the proposed controller, it is expected to obtain a sinusoidal current at the output of the inverter with a variable amplitude that will depend on the modulation index of the amplitude.

***Table 1. Characteristics of the solar panel.***

| Characteristics of the solar panel | |
|---|---|
| *Maximum Power PM (W)*(±3%) | 50 W |
| *Maximum Voltage Vm (V)*(±3%) | 17.9 V |
| *Maximum Current Imp (A)*(±3%) | 2.79 A |
| *Open Circuit Voltage Voc (V)* | 22.1 V |
| *Short Circuit Current Isc (A)* | 3.96 A |
| Maximum System Voltage | 600 V |

In Figure 4, the simulation in MATLAB/Simulink of the solar panel with the characteristics outlined in Table 1 is shown. The solar panel is configured with a temperature of 25°C and a solar radiation of 1000 W/m². Considering a 6 Ω resistor connected to the solar panel, which acts as a load, the aim is to visualize the voltage and current described in the previous table.

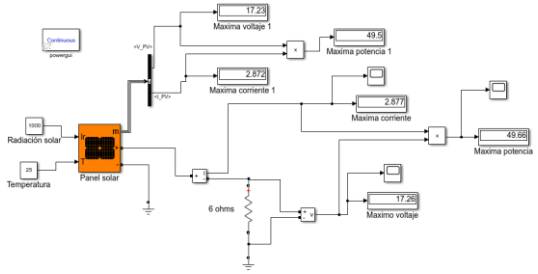


Figure 4. Simulation of the solar panel.

Taking into account the characteristics outlined in Table 1, the connection of the solar panels in series was carried out as shown in Figure 6, to obtain the desired input voltage for the photovoltaic system.

This connection was made to display the voltage, current, and power supplied by the ten photovoltaic panels, which were used to provide energy to the photovoltaic system.

- The variable radiation of {1000-1500-500-1000} W/m² and a temperature of 25 °C is shown in the red box. The connection of the solar panels is expressed in the subsystem of the yellow box.
- The outputs of voltage, current, and power are observed in the black box.

Table 2 shows the theoretical and simulated results of the solar panel with solar radiation of 1000 W/m² and a temperature of 25 °C. This test aims to demonstrate the variations that exist in the solar panel.

Table 2. Response of the solar panel for voltage, current, and power..

| Connection of solar panels | | | |
|---|---|---|---|
| Parameters. | Theoretical. | Simulated. | % error |
| Voltage. | $Vp = 179\ V$ | $Vp = 178.8\ V$ | 0.11 % |
| Current. | $I = 2.79\ A$ | $I = 2.793\ A$ | *0.11*% |

## 5. Design of Power Electronic Converters

In this phase, the design of the converters in the system is presented. Table 3 shows the parameter values for the buck converter, inverter, and the resistive-inductive load.

Table 3. Proposed Values for the Buck Converter, Inverter, and Resistive-Inductive Load

| Element | Value |
|---|---|
| | Buck Converter |
| Inductor | $L = 679.68\ \mu H$ |
| Capacitor | $C = 450\ \mu F$ |
| Switching frequency | $f_s = 50\ kHz$ |
| | Inverter |
| Switching Frequency | $f_s = 15\ kHz$ |
| | Load |
| Inductor | $L_0$ =10 mH |
| Internal Resistance of the Inductor | $R_0$ =0.7 Ω |
| Load Resistance | $RL$ =100 Ω |

In Figure 5, the circuit of the photovoltaic system in MATLAB/Simulink is presented based on the design parameters outlined in Tables 2 and 3.

## 6. Design of Active Disturbance Rejection Control in the MATLAB/Simulink Environment

Once the mathematical analysis of the photovoltaic system and the Active Disturbance Rejection Control (ADRC) has been carried out, the design of the photovoltaic system is implemented by applying ADRC in the MATLAB/Simulink environment. Figure 6 shows the ADRC controller.

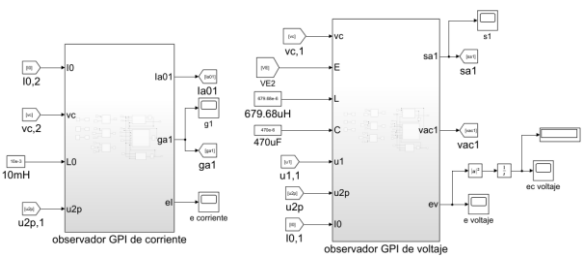

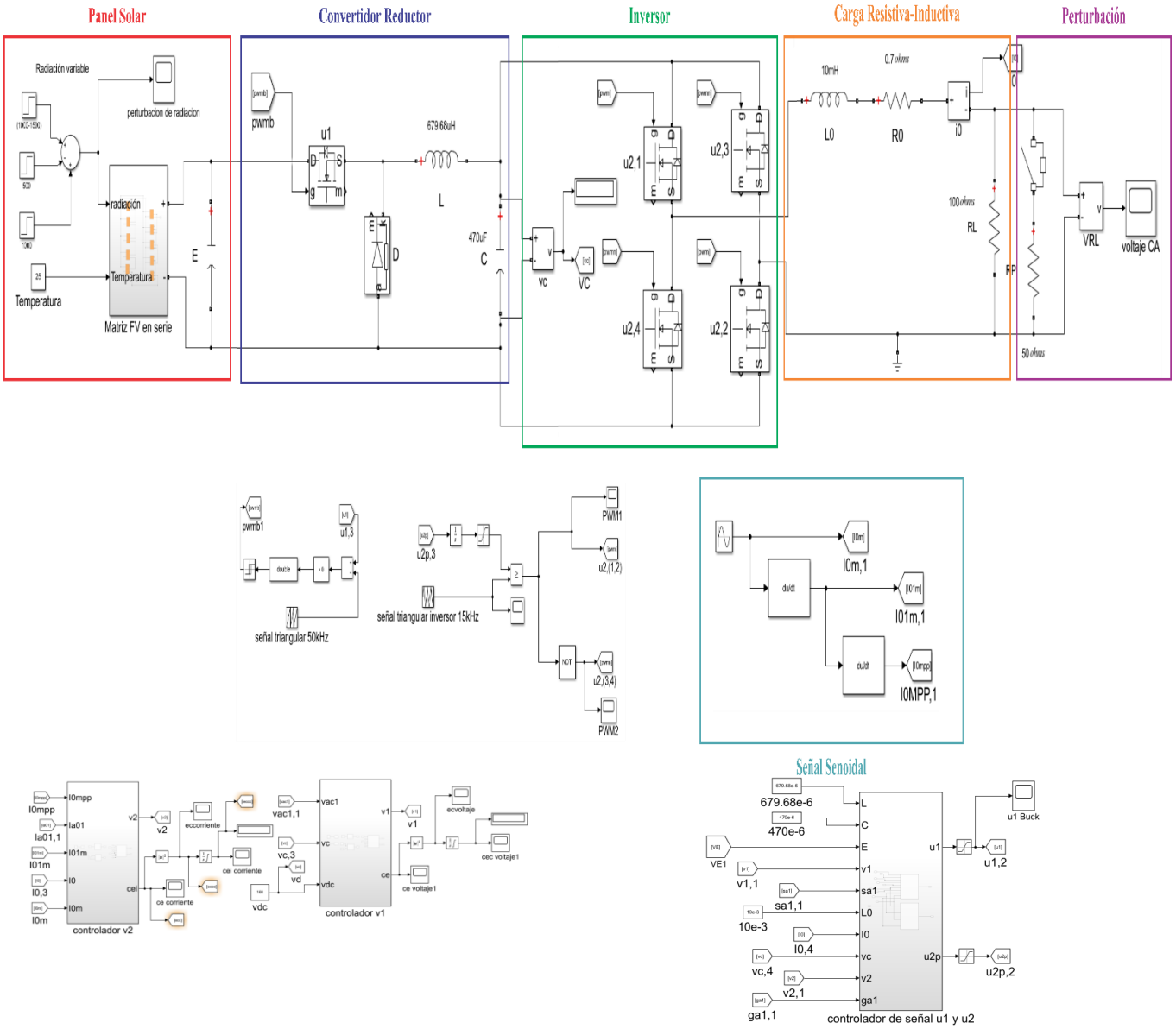


Figure 6. ADRC in MATLAB/Simulink.

Figure 5. Design of the photovoltaic system in MATLAB/Simulink

The GPI voltage observer corresponding to the set of equations (17) was tuned using the set of equations (20), resulting in $\zeta_1 = 0.7071$, $\omega_{n1} = 10000$, and $\alpha = 6000$.

The GPI current observer corresponding to the set of equations (19) was also tuned using the set of equations (21), yielding $\zeta_{11} = 0.7071$, $\omega_{n11} = 12000$, and $\alpha = 6000$.

The auxiliary controller $v_1$ corresponding to the set of equations (22) was selected with the desired reference voltage $V_l$ at the output of the buck converter, which was tuned using the set of equations (24), resulting in $\zeta_2 = 0.7071$ and $\omega_{n2} = 1000$. The auxiliary controller $v_2$ corresponding to the set of equations (23) was similarly tuned using equations (25), resulting in $\zeta_3 = 0.7071$ and $\omega_{n3} = 7000$.

## 7. Simulation Results

To assess the robustness of the ADRC controller, a variable solar radiation of {1000-1500-500-1000} W/m² and a temperature of 25 °C are considered, along with an external load resistance applied at 0.5 s. Figure 7 shows the voltage provided by the solar panel applied to the buck converter, with a 470 µF capacitor included to reduce the generated ripple.

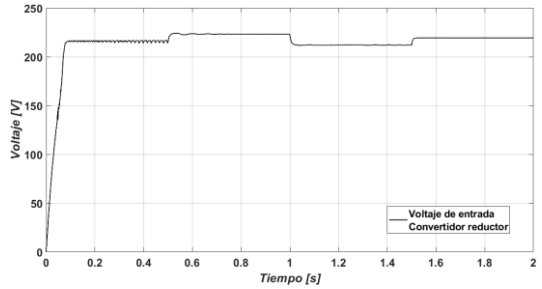


Figure 7. Output Voltage of the Solar Panel.

Next, figure 8 presents the control signal u1u_1u1 generated by the ADRC controller for the buck converter. The control signal reacts to the disturbances generated in the solar panel and the load; this self-adjustment is performed to compensate for the variation in voltage.

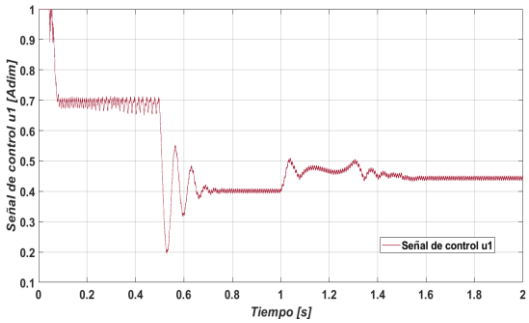


Figure 8. Control signal u1 for the buck converter applying ADRC.

In Figure 9, the PWM signal responsible for activating the switching device of the buck converter is shown, generated by comparing a triangular signal at 50 kHz with the signal u1 produced by the same controller.

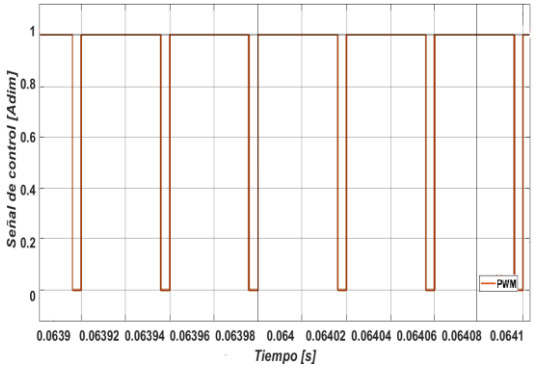


Figure 9. PWM Modulation for the Buck Converter Applying ADRC.

In Figure 10, the control signal u2 generated by the ADRC controller for the inverter is shown. This signal decreases when the load starts operating at 0.5 seconds, as it compensates for the increase in current generated by the inverter load

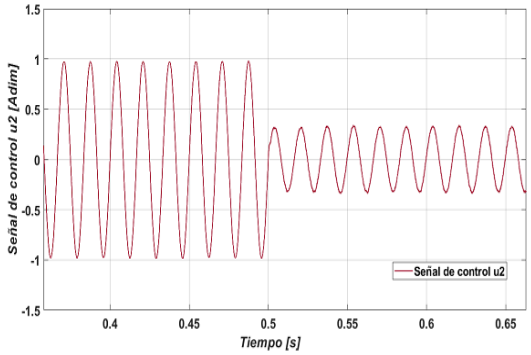


Figure 10. Control signal u2 for the inverter applying ADRC.

Figure 11. Control signal for the switching devices for bipolar PWM modulation in the inverter, generated by comparing a triangular signal of 15 kHz and the signal u2 generated by the controller.

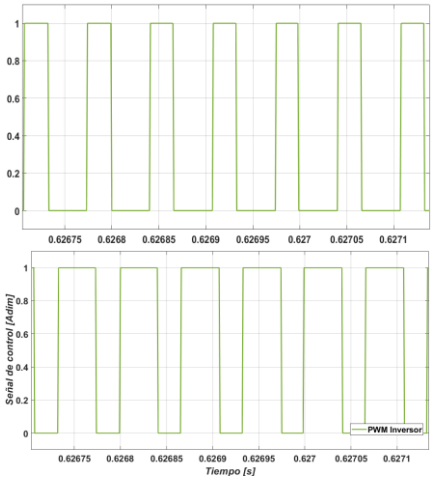


Figure 11. Bipolar PWM modulation for the inverter applying ADRC.

Next, the simulation results of the photovoltaic system are presented, considering an input voltage to the buck converter provided by the solar panel $V_p = 170\,V$, a desired voltage in the buck converter $V_{ref} = 160\,V$, and a desired sinusoidal current with a peak amplitude $I_d = 1.5\,A$ in the inverter.

Figure 12 shows the output voltage in the buck converter, where the settling time is 0.1 s applying the ADRC. It is worth mentioning that for the controller tuning, the trial and error technique is used, where the gains are initially set to 0, and then the values are slowly increased to a specific value until the output signal exhibits good behavior. The figure shows a voltage mismatch due to the disturbances introduced in the load and variations in solar radiation; however, it manages to maintain the desired voltage reference.

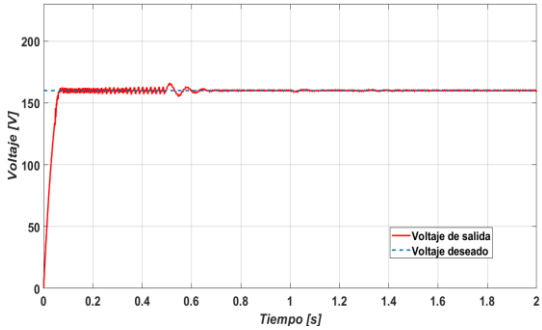


Figure 12. Output voltage of the buck converter Vref=160V applying ADRC.

In figure 13, the behavior of the output sinusoidal signal from the inverter is shown with a desired peak current amplitude $I_d = 1.5\,A$. The same figure displays the current signal from the inverter, with a settling time of 0.1s when applying the ADRC controller. It is worth mentioning that the same trial and error technique used for voltage tuning was employed for tuning the controller gains.

To better understand the quality of the output current from the inverter, the FFT Analysis tool in MATLAB/Simulink is utilized to obtain the amplitude of the fundamental component (60 Hz) and the Total Harmonic Distortion (THD) of the current before the disturbance acts on the load figure 14 shows a current with a fundamental component of 1.537ª and a THD of 8.93% when applying the ADRC controller.

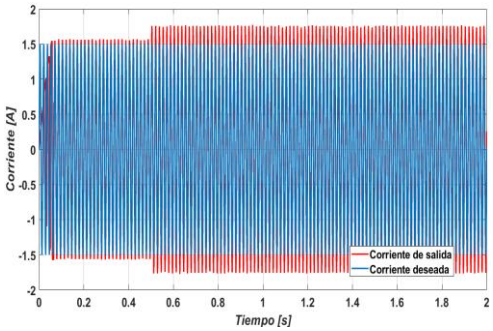


Figure 13. Output current in the inverter Id=1.5A applying ADRC.

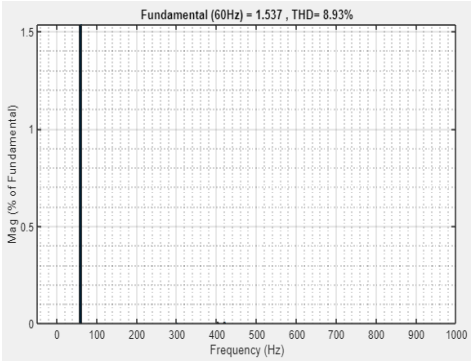


Figure 14. Fundamental component at (60 Hz) = 1.537 A and total harmonic distortion (THD) = 8.93% before the disturbance applying ADRC.

In figure 15, a "zoom" view is presented to better observe the current of the inverter when the load disturbance occurs at 0.5 s. There is an increase in the current ripple at the output of the inverter due to the sudden application of the external resistance in parallel with the load resistance.

To evaluate the quality of the output current from the inverter, the amplitude of the fundamental component (60 Hz) and the total harmonic distortion (THD) of the current during the disturbance are obtained. In figure 16, the current shows a fundamental component of 1.512 A and a total harmonic distortion (THD) of 13.73%. As can be observed, the ADRC controller has a closer approximation to the desired current.

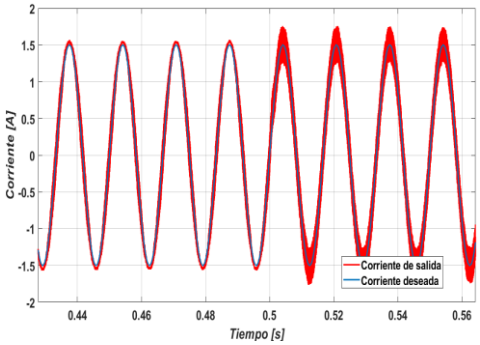


Figure 15. Disturbance applied at 0.5 s in the current of 1.5 A applying ADRC.

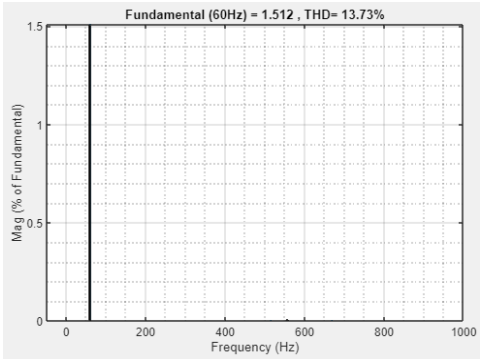


Figure 16. Fundamental component at (60 Hz) = 1.512 A and total harmonic distortion (THD) = 13.73% after the disturbance applying ADRC.

Figure 17. The output voltage of the inverter is sinusoidal with an amplitude $V_{inv} = 150\ V$ and a $V_{rms} = 106\ V$. The disturbance that occurs at 0.5 s causes the 100 Ω load resistor to be in parallel with the external 50 Ω resistor, resulting in a decrease in the output voltage of the inverter to $V_{inv} = 50\ V$. The voltage does not remain stable because the control is not robust in voltaje.

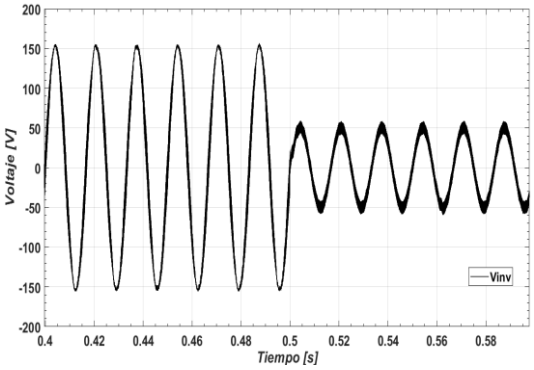


Figure 17. Output voltage of the inverter Vinv = 150 V applying ADRC.

In figure 18, the voltage error signal in the buck converter generated by the controller is presented. It is important to mention that this error tends to 0 V. Next, the squared error is obtained, as shown in figure 19, and the integral of the squared error (ISE) is shown in figure 20. These values are obtained because both voltage responses exhibit overdamping, causing an increase in the ISE for each controller.

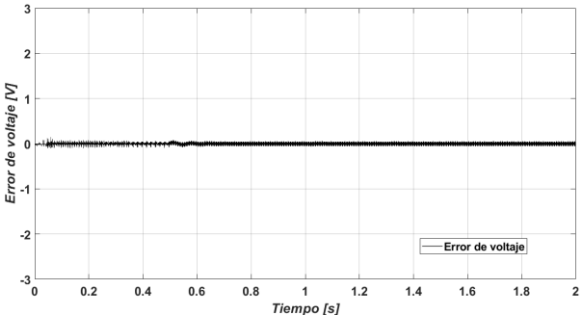


Figure 18. Voltage error in the buck converter applying ADRC.

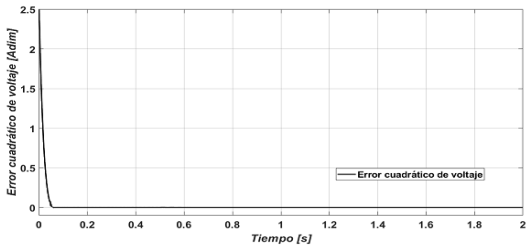


Figure 19. Squared voltage error in the buck converter applying ADRC

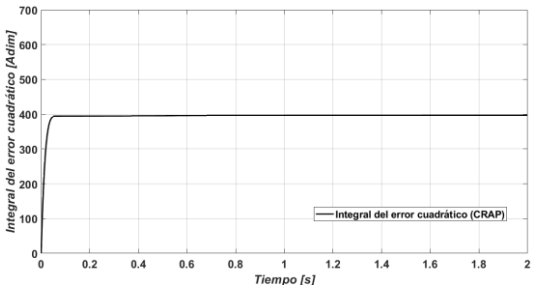


Figure 20. Integral of the squared voltage error in the buck converter applying ADRC.

In Figure 21, the current error signal in the inverter is shown; the value of this signal is approximately equal to 0 A. Similarly, the squared error signal is obtained, as shown in Figure 22, along with the signal of the integral of the squared error (ISE), as depicted in Figure 23.

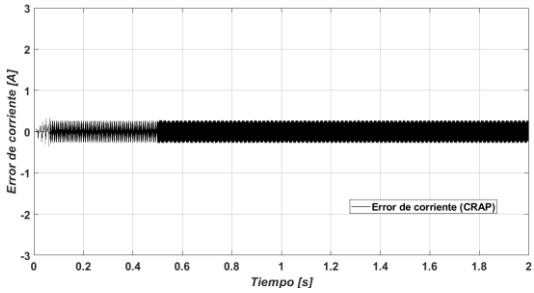


Figure 21. Current error in the inverter applying ADRC.

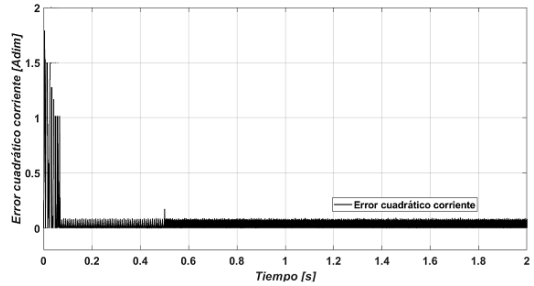


Figure 22. Squared current error in the inverter applying ADRC.

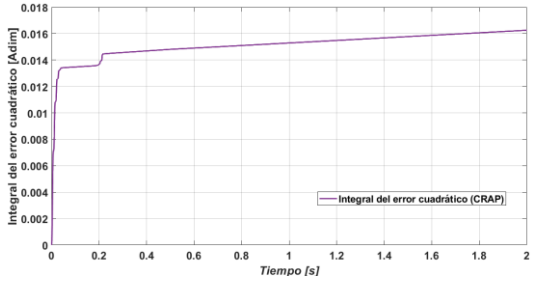


Figure 23. Integral of the squared current error in the inverter applying ADRC.

## 8. Conclusion

This work involved the design and simulation of a photovoltaic system applying the ADRC controller, which fulfills the following tasks: regulating the output voltage of the buck converter and tracking a sinusoidal reference current at the output of the inverter. It is important to mention that first, the mathematical modeling of the photovoltaic system was performed using Kirchhoff's laws, followed by the design of the active disturbance rejection control, and then the corresponding simulation was carried out using MATLAB/Simulink.

The simulation results obtained demonstrate the effectiveness and robustness of the active disturbance rejection control, where it is generally observed that the desired voltage is achieved at the output of the buck converter, and the sinusoidal current reference is followed at the output of the inverter, despite variations in the input voltage and the external disturbance applied to the load. Additionally, the simulation results show that with the property of differential flatness and the active disturbance rejection control law, the estimation error of the output voltage of the converter and the load current can be brought to zero to achieve the desired output voltage and the desired reference current. The same results indicate a good dynamic response of the ADRC with a settling time of less than 0.1 s, a fundamental component (60 Hz) of 1.53 A, and lower current distortion at the output of the inverter with a THD of 8.93% before the disturbance, as well as a fundamental component of 1.51 A and a THD of 13.73% during the disturbance.

## References

[1] International Renewable Energy Agency, Renewable Energy Cost Analysis - Solar Photovoltaics, IRENA, Insights, Vol. I, No. 4, pp. 1-45, 2012.

[2] Guerrero Ramírez E, Martínez Barbosa A, Contreras Ordaz M. A, Guerrero Ramírez G, Guzmán Ramírez G, Barahona Avalos J.L, Adam Medina M. Technological University of the Mixteca, National Center for Research and Technological Development, Energies. pp. 5-6. 2022.

[3] Guerrero Ramírez E, Martínez Barbosa A, Contreras Ordaz M. A, Guerrero Ramírez G. Technological University of the Mixteca, National Center for Research and Technological Development, Electrical Energy Systems. pp. 2-3. September 20, 2019.

[4] Hart W. D. Power Electronics, Madrid: Pearson Education, 2001.

[5] Morales Laguado L, Chomorro H, Soriano J. Analysis and Comparison between a Fuzzy PI Controller and a Conventional Optimal PI Controller for a Buck Converter, Engineering and Research, Bogotá, December 2009.

[6] Navarro D, Barajas A, Pérez E, Cortes D. Extension of DC/DC Controllers to DC/AC Implemented by Sliding Modes or SPWM. October 2013.

[7] Montes Aguilar J.G, Conditioning of an Inverter through a Proposal for an Auxiliary Audiovisual System for Indigenous Communities, Center for Research in Advanced Materials, S.C, Ciudad Juárez, Chihuahua, pp. 9-11, April 2014.

[8] Vázquez Gutiérrez R.A, Design and Implementation of a Low-Cost 500VA Single-Phase Inverter, Technical School of Engineering and Telecommunications Systems, pp. 25-27.

[9] Han J. From PID to Active Disturbance Rejection Control. IEEE on Industrial Electronics, Vol. LVI, No. 3, pp. 900-906. 2009.

[10] Johnson C.D. Accommodation of External Disturbances in Linear Regulator and Servomechanism Problems, IEEE Transactions on Automatic Control, Vol. XVI, No. 6, pp. 635-644, 1971.

[11] Sira Ramírez H, Luviano Juárez A, Cortés

Romero J. Robust Linear Control of Differentially Flat Nonlinear Systems. Ibero-American Journal of Automation and Industrial Information, Vol. VIII, No. 1, pp. 14-28. 2011.

[12] Sira Ramírez H, Agrawal S.K. Differentially Flat Systems, USA: CRC Press. 2004.

[13] Fliess M, Lévine J, Martin P, Rouchon P. On Differentially Flat Nonlinear Systems, Paris, France: C. R. Acad. Sci. 1992.

[14] Esteva Pérez R, Design and Simulation of Active Disturbance Rejection Control for the Buck Converter-Inverter System: For Photovoltaic Applications. Technological University of the Mixteca. February 2023.

[15] [1Guerrero E, Sira H, Martínez A, Linares J, Guzmán E. On the Robust Control of Parallel-Cascade DC/DC Buck Converter. IEEE LATIN AMERICAN TRANSACTIONS, Vol. 14, February 2016.

[16]PRO-5012 Catalog, epcom power line: energy solutions